

Validity of Cosmic String Pattern Search with Cosmic Microwave Background

E. Jeong¹ and G. F. Smoot^{1,2}

¹Department of Physics, University of California, Berkeley, CA, 94720

²Lawrence Berkeley National Laboratory, 1 Cyclotron Road, Berkeley, CA, 94720

(Dated: February 7, 2020)

We introduce a new technique to detect discrete temperature steps from cosmic strings left on Cosmic Microwave Background (CMB) anisotropy map. The detecting power of the technique is only constrained by two unavoidable features of CMB data: (1) finite pixelization of sky map and (2) Gaussian fluctuation from instrumental noise and primordial anisotropy. We set the upper limit on cosmic string parameter as $G \cdot 3.7 \cdot 10^{-6}$ at 95% CL and find that the magnitude of temperature step has to be greater than 44 K in order to be detected for Wilkinson Microwave Anisotropy Probe (WMAP) data set.

PACS numbers: Valid PACS appear here

I. INTRODUCTION

Physicists at the frontier of high energy physics are now trying to increase our understanding of the Nature to an energy level as high as the Planck scale (10^{19} GeV) while experiments have paved road up to 10^3 GeV scale. There is no reason to expect that terrestrial accelerators would fill the huge gap lying between current status of experiment and theory. Therefore, physicists have turned to the early universe hoping to discover observational/experimental evidences for pioneering theories. Cosmic strings is one of the hottest topics, whose discovery will probably be an important landmark on the way to the Planck scale. Cosmic strings have many attractive features over other topological defects in the matter of its existence. One of the examples is that cosmic strings do not result in the overclosure of universe while other defects do. The quest for cosmic strings has been performed in two ways: statistical method and direct search for individual cosmic string. Many studies on statistical side agreed that the contribution from cosmic strings to statistical observables such as power spectrum is at most 10% [1, 2, 3, 4, 5], meaning that cosmic strings played, if any, a minor role in making the universe as it is. On the other hand, a candidate suspected to be a double image formed by a cosmic string turned out to be two neighboring galaxies [6] and failed in discovering cosmic strings directly. Other workers have set upper limits on the cosmic string parameter [7, 8, 9, 10, 11, 12, 13]. CMB anisotropy maps could contain unique signals created by cosmic strings, discrete temperature steps due to Kaiser-Stebbins effect [4, 15]. But those are probably obscured by instrumental noises and other physical structures of anisotropies. In this letter, we introduce a technique to estimate how strong a signal from cosmic strings has to be in order to be identified unequivocally. We calibrate the detecting power of this technique by applying it to simulated anisotropy maps based on a reasonable modeling. In the sense that our new technique works perfectly when background Gaussian fluctuation is

turned on, we explicitly show the inherent limitations of CMB anisotropy map as a site for cosmic string search and explain a feasible way to improve the detecting power of the algorithm. In the last part of this letter, we apply this method to WMAP 3-year W-band data set [16] and analyze the implication of the results.

II. MODELING AND SIMULATION

Cosmic strings are believed to evolve over time by reconnecting, intercommuting and evaporating since their birth [15]. According to computer simulations e.g [17], tens of long strings with cosmological length can survive up to time of recombination within the volume of observable universe. Correlation length, $\langle t \rangle$, of a cosmic string can be estimated most conservatively as $\langle t \rangle \approx ct$ and a cosmic string does not develop much wiggle within correlation length. At the time of recombination, the angular size of horizon for the most preferred CDM model becomes $1:8$. We consider a square patch of CMB anisotropy sky map ($N \times N$ pixels) that extends to a size of horizon at the time of recombination so that the conic space-time formed by a cosmic string can be effected within the region. Then, a square patch of CMB anisotropy sky map that contains a segment of moving cosmic string can be decomposed into three parts as illustrated in Figure 1: (1) uniform background temperature (T_0) in a CMB anisotropy map, (2) Gaussian fluctuation (variance σ_G^2) and (3) discrete temperature step from a moving cosmic string. The uniform background temperature T_0 comes from super-horizon scale primordial fluctuations. Because we pick a horizon-sized region, the super-horizon fluctuations will appear to be a constant temperature shift for the whole patch. Smaller scale (sub-horizon) fluctuations and instrumental noise add up incoherently to form a Gaussian fluctuation within the square and since they are uncorrelated, the variance of combined Gaussian signal becomes $\sigma_G^2 = \sigma_{CMB}^2 + \sigma_{noise}^2$ where σ_{CMB}^2 and σ_{noise}^2 are variances for fluctuations of primordial origin and instrumental noise respectively.

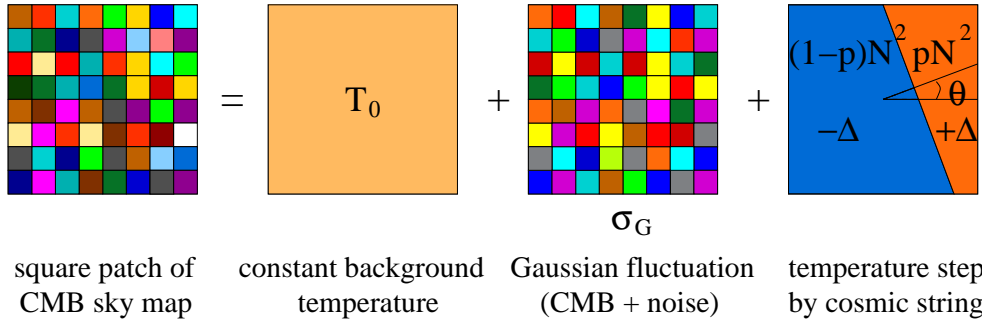


FIG. 1: A decomposition of sky map patch. The square patch is decomposed into uniform background temperature (T_0) + Gaussian fluctuation + discrete temperature step. The number of pixels in a patch is N^2 .

The discrete temperature step produced by a moving cosmic string is described by the analytic expression [14],

$$= 4 G s T \hat{n} (\hat{v} \cdot \hat{s}) \quad (1)$$

where \hat{n} represents the half-height of temperature step given in Figure 1 and $T = 2.725\text{K}$ is the universal background temperature of CMB. \hat{v} and \hat{s} are direction vectors for the line of sight, velocity of string segment and direction of string segment respectively.

$s = (1 - \frac{2}{s})^{1/2} = (1 - (v=c)^2)^{1/2}$ is the Lorentz factor involved with motion of string. G is the dimensionless cosmic string parameter where G is the gravitation constant and s is the linear energy density of cosmic string. Here we introduce five parameters that characterize a square patch of string embedded sky map, T_0 , σ_G , p (blue-shifted pixels/total pixels) and θ (orientation of step). We concoct a simulated patch of CMB anisotropy map by assigning arbitrary legitimate values to the parameters and adding the three components illustrated in Figure 1. To recover these parameters from the CMB anisotropy map where the step patterns are intermixed, we employ five observables which can be expressed in terms of $(T_0, \sigma_G, p, \theta)$:

$$\text{mean} : = \frac{1}{N^2} \sum_j T_j; \quad j = \text{allpixels} \quad (2)$$

$$\text{dipole moment} : x = \frac{1}{N^3} \sum_j T_j x_j; \quad (3)$$

$$y = \frac{1}{N^3} \sum_j T_j y_j \quad (4)$$

$$\text{inertia} : = \frac{4}{N^3} \sum_j T_j \mathbf{x}_j \mathbf{x}_j \quad (5)$$

$$X_j = (x_j x + y_j y) =$$

$$\text{variance} : = \frac{1}{N^2} \sum_j (T_j - \bar{T})^2 \quad (6)$$

where \bar{T} is the magnitude of dipole moment. We choose the orientation of temperature step $\theta = 0$ without loss of generality since it gives especially simple analytic forms of observables introduced in (2)–(6). In the absence of

Gaussian background fluctuation ($\sigma_G = 0$), the observables are expressed as

$$= T_0 + (2p - 1) \quad (7)$$

$$x = p(1 - p) \quad (8)$$

$$y = 0 \quad (9)$$

$$= T_0 + (2p - 1) \frac{2p - 1}{2} \quad (10)$$

$$^2 = 4^2 p(1 - p); \quad (11)$$

and we recover the characteristic parameters perfectly,

$$p = \frac{2}{4} \frac{\frac{1}{2} (j - j+)}{j - j} \quad (12)$$

$$= \frac{(j - j - 4)^2}{2 (2 - j - j)} \quad (13)$$

$$T_0 = (2p - 1) \quad (14)$$

$$= \tan^{-1} \frac{y}{x} = 0 \quad (15)$$

$$G = 4^2 p(1 - p)^{\frac{1}{2}} = 0; \quad (16)$$

On the other hand, when the background fluctuation is turned on, what we expect to get back are unbiased estimates plus Gaussian errors with variance σ_i^2 ($i = T_0, \sigma_G, p, \theta$),

$$p_{\text{obs}} = p + \sigma_p \quad (17)$$

$$x_{\text{obs}} = \bar{x} \quad (18)$$

$$T_{0,\text{obs}} = T_0 + \sigma_{T_0} \quad (19)$$

$$y_{\text{obs}} = \bar{y} \quad (20)$$

$$\sigma_{\text{obs}} = \sigma_G + \sigma_{\sigma_G}; \quad (21)$$

The errors ($\sigma_p, \sigma_{T_0}, \sigma_{\sigma_G}$) present in (17)–(21) are measures how precisely a temperature step screened by background fluctuation is recovered. Figure 2 shows the behaviors of error as functions of θ for three different pixel numbers for a patch. The variance of the background fluctuation chosen here is the average variance of patches with angular radius $R = 1.8^\circ$ for WMAP 3-year W-band data set with Kp2-mask applied [16]. The most pronounced feature of the graphs is that the er-

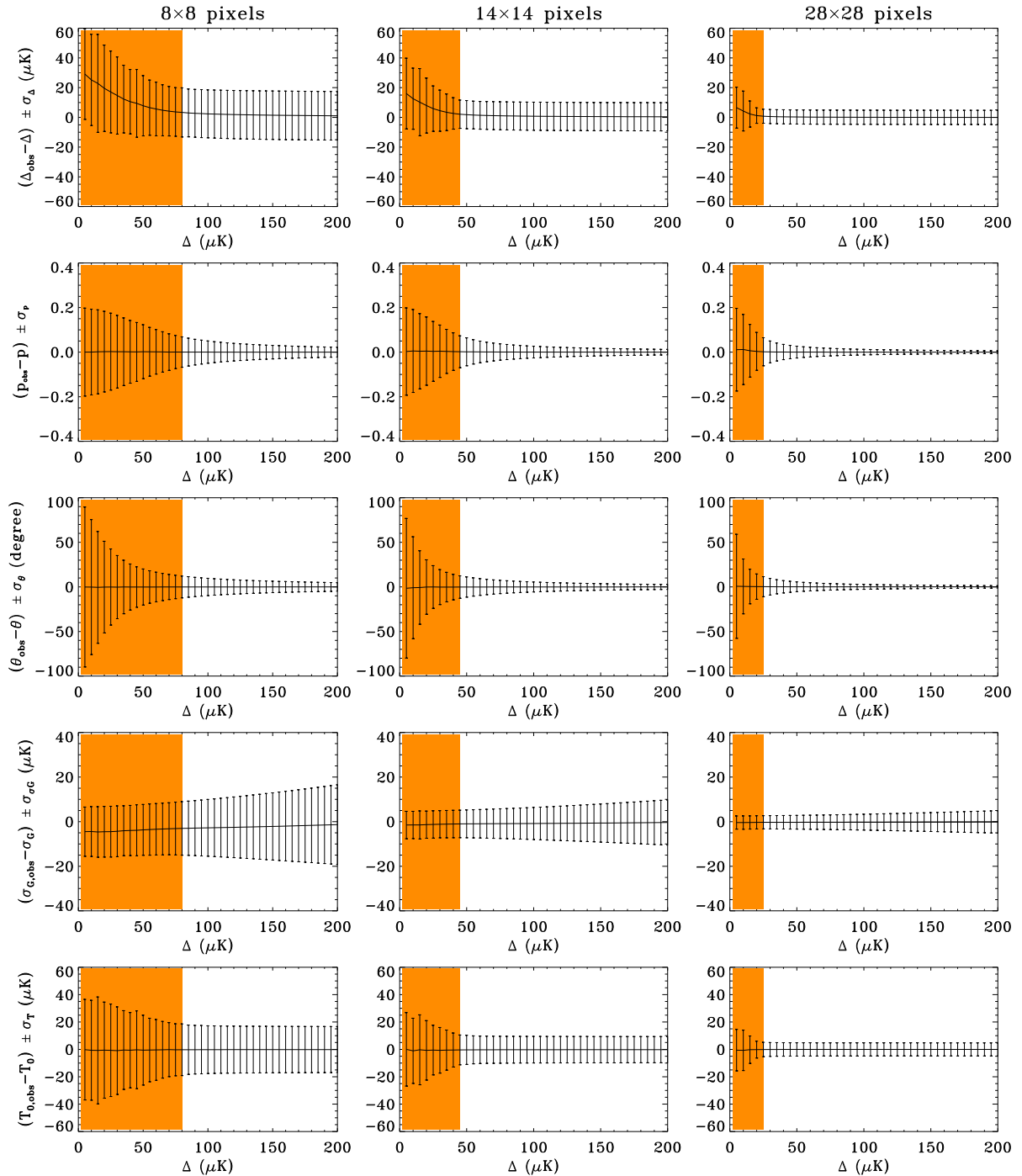


FIG. 2: Evolution of errors of characteristic parameters obtained in (12)–(16) as functions of Δ with fixed values of parameters ($T_0 = 10.0$ K; $p = 0.5$; $\theta = 0$; $\sigma_0 = 116.0$ K). Left panels: 8 \times 8 pixels in a square, middle panels: 14 \times 14 pixels, right panels: 28 \times 28 pixels. For each size of patch, the number of simulations performed is 10,000. Orange (shaded) regions indicates the ranges of Δ for which the step feature in a patch is not obvious compared to its background fluctuation ($\sigma_0 = 116.0$ K). The result on θ is biased upward because the simulations with erroneous values of θ ($\theta < 0$) were not included in the statistics.

rror bars are wildly undulating while stays small compared to background fluctuation σ_0 with converging envelopes as Δ increases. From this feature, we see that our algorithm to extract the characteristic parameters works poorly for low temperature steps compared to

background fluctuation such as 90 error on orientation estimate. Even breakdowns of algorithm do happen in the orange (shaded) region, resulting in erroneous parameter values such as negative θ or p not in the range between 0 and 1. Simulations with collapsed re-

TABLE I: Simulation results at the critical values of ϵ above which good results on parameter recovering begin to come out.

| patch | parameter | input | computed (1) | |
|---|-------------|-------|--------------|-------|
| 8 8 pixels $g = 116.0 \text{ K}$ $= 80.0 \text{ K}$ | (K) | 80.0 | 83.35 | 16.55 |
| | P | 0.5 | 0.50 | 0.07 |
| | (degree) | 0.0 | 0.07 | 12.25 |
| | g (K) | 116.0 | 112.98 | 12.0 |
| | T_0 (K) | 10.0 | 9.73 | 18.90 |
| 14 14 pixels $g = 116.0 \text{ K}$ $= 45.0 \text{ K}$ | (K) | 45.0 | 47.12 | 9.53 |
| | P | 0.5 | 0.50 | 0.07 |
| | (degree) | 0.0 | 0.17 | 12.63 |
| | g (K) | 116.0 | 115.00 | 6.17 |
| | T_0 (K) | 10.0 | 9.62 | 10.87 |
| 28 28 pixels $g = 116.0 \text{ K}$ $= 25.0 \text{ K}$ | (K) | 25.0 | 25.77 | 4.71 |
| | P | 0.5 | 0.50 | 0.06 |
| | (degree) | 0.0 | 0.24 | 11.23 |
| | g (K) | 116.0 | 115.71 | 2.96 |
| | T_0 (K) | 10.0 | 9.90 | 5.25 |

sults are not included in the statistics shown in Figure 2 since those cases are evidently the ones with insufficiently strong signals against background fluctuation. As the temperature step gets higher, we begin obtaining the computed parameters very close to the true values with acceptable errors (dubbed "good" results) and it allows us to recover the temperature step parameters faithfully. It is easily found from Figure 2 that the patches with more pixels work better for they have faster attenuation of uncertainties and errors are smaller. Table I displays the performances of the algorithm for the values of ϵ at the borders above which errors for temperature step (Δ) do not get any better. We use circular patches for WMAP data analysis rather than square patches because of computational advantage. Algebraic expressions for observables for given in (7)–(12) work very well for circular patches with negligible numerical differences with square patches. A square patch with 28 28 pixels at the normal resolution of WMAP data (3,145,728 pixels for full sky) covers nearly the same area as the circular region with angular radius $R = 1.8^\circ$. Thus, when there is a moving cosmic string passing through the center of the patch, all pixels in the patch will be affected by conic space-time formed by the cosmic string. If a cosmic string is placed between the last scattering surface and the Earth ($0 < z < 1100$), the step pattern should be larger than the size of the patch. We performed further detecting power test with 28 28 pixels patches and found the critical value of ϵ_c , above which "good" results start to come out is related to the background fluctuation g by

$$\epsilon_c' \approx \frac{1}{4} g : \quad (22)$$

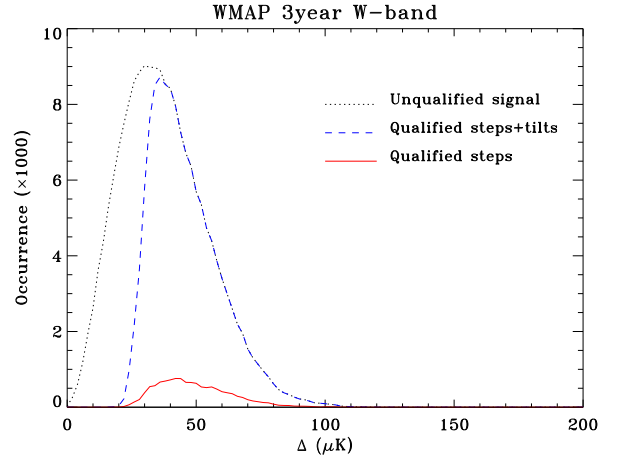


FIG. 3: Distributions of detected in WMAP 3-year W-band data set. Number of spots-unqualified signal (dotted): 193,160, qualified step+tilt (dashed): 129,049, qualified step (solid): 12,330.

III. APPLICATION TO WMAP

An observed CMB anisotropy map is an aggregate of various independent modes of perturbation ranging from tiny sub-horizon scales to super-horizon scales well beyond the correlation length. As illustrated in Figure 1, fluctuations with larger or smaller scales compared to the size of a test patch are neatly prescribed. But, the intermediate scales whose wavelengths are comparable to the size of test patch will appear to be continuous temperature tilts which also give plausible values of step parameters. One drawback of this algorithm is that it does not distinguish a discrete temperature step and a smooth temperature slope. However, this shortcoming can be easily fixed: if an apparent temperature step is detected at a spot (center of a patch) in the map, we repeat the analysis with half-sized patch at the same spot. If the structure is a continuous slope, then it would return a half the value of than previous result while for the signal from a discrete step, the returned should stay the same with in error. We consider only the patches with $p = 0.5$ to avoid multiple count on the same pattern. We conducted the step signal search through the WMAP 3-year W-band data set and found 193,160 unqualified signals against background fluctuation (the constraint in (22) is not applied), 129,049 qualified steps+tilts (signals that meet the constraint (22)) and 12,330 qualified discriminated steps. The of qualified steps ranges

$$(18.3 \text{--} 3.0) \text{ K} < \epsilon < (115.4 \text{--} 6.0) \text{ K} : \quad (23)$$

as the histograms are shown in Figure 3. Patches with radius $R = 1.8^\circ$ in WMAP 3-year W-band have background fluctuation g less than 176 K in the Kp2-mask cleared region. This means, at the worst case, we can identify a step signal as low as 176 K = $4 = 44$ K with moderate errors. Therefore, if there are cosmic string

signals with 115.4 K and they are located on the available region (out of Galactic plane or $Kp2$ masked region), they would not be missed. Thus, we can set an upper limit on cosmic string signal

$$= 4 \text{ G} \quad s \text{ sT} \cos \theta < 127.4 \text{ K} ; \quad 95\% \text{ CL} \quad (24)$$

where θ is arbitrary. Thus, with $h_{\text{ss}} \approx 1$ [15], the upper limit of cosmic string parameter can be estimated as

$$G \approx 3.7 \times 10^{-6} ; \quad 95\% \text{ CL} \quad (25)$$

Acknowledgments

Computer simulation and data analysis with WMAP data set were done using the HEALPix [18, 19]. This work was supported by LBNL and the Department of Physics at University of California, Berkeley.

[1] L. Pogosian et al., Observational Constraints on Cosmic String Production During Brane Inflation [Phys. Rev. D 68, 023506, 2003].

[2] J.-H. Wu, Coherence Constraint on the Existence of Cosmic Effects (astro-ph/0501239, 2005).

[3] A. Fraisse, Constraints on Topological Effects Energy Density from First-Year WMAP Results (astro-ph/0503402, 2005).

[4] A.-C. Davis and T. Kibble, Fundamental cosmic strings (hep-th/0505050, Contemp. Phys. 46 313–322, 2005).

[5] M. Wyman et al., Bounds on Cosmic Strings from WMAP and SDSS [Phys. Rev. D 72, 023513, 2005].

[6] E. A. gol et al., Hubble Imaging Excludes Cosmic String Lens (astro-ph/0603838, 2006).

[7] M. Hindmarsh, Small scale microwave background fluctuations from cosmic strings (astro-ph/9307040, Astrophys. J. 431: 534–542, 1994).

[8] L. Perivolaropoulos and N. Simatos, Hints of Cosmic String Induced Discontinuities in the COBE Data? (astro-ph/9803321, 1998).

[9] E. Jeong and G. F. Smoot, Search for Cosmic Strings in CMB Anisotropies (astro-ph/0406432, Astrophys. J. 624: 21–27, 2005).

[10] A. S. Lo and E. L. Wright, Signatures of Cosmic Strings in the CMB (astro-ph/0503120, 2005).

[11] U. Seljak and A. Slosar, B polarization of cosmic microwave background as a tracer of strings (astro-ph/0503120, Phys. Rev. D 74, 063523, 2006).

[12] L. Pogosian et al., On vector mode contribution to CMB temperature and polarization from local strings (astro-ph/0604141, 2006).

[13] A. Fraisse, Limits on SUSY GUTs and Effects Formation in Hybrid Inflationary Models with Three-Year Wilkinson Microwave Anisotropy Probe (WMAP) Observations (astro-ph/0603589, 2006).

[14] N. Kaiser and A. Stebbins, Microwave anisotropy due to cosmic strings (Nature 310: 391–393, 1984).

[15] A. Vilenkin and E. P. S. Shellard, Cosmic Strings and Other Topological Effects (Cambridge University Press, UK, 1985).

[16] <http://lambda.gsfc.nasa.gov/product/map/>.

[17] http://www.damtp.cam.ac.uk/user/gr/public/cs_evol.htm

[18] <http://healpix.jpl.nasa.gov>.

[19] K. M. Gorski et al., HEALPix: A Framework for High-Resolution Discretization and Fast Analysis of Data Distributed on the Sphere [Astrophys. J. 622: 759, 2005].